Field Simulation of Dipole Antennas for Interstitial Microwave Hyperthermia

Gerd Schaller, Jurgen Erb, and Rainer Engelbrecht

Abstract— **The electromagnetic field of dipole antennas for interstitial microwave hyperthermia is investigated using a finite integration algorithm program. The numerical method is applied to conventional, clinically used applicators and is also used for the improvement and optimization of sophisticated applicators, e.g., in a triaxial technique. Simulations of the frequency dependent impedance match, the E-field and the specific absorption rate (SAR) distribution of different applicators immersed in a muscle phantom are presented and compared with measurements. Moreover, results for arrays of two and four applicators are given. The field simulation allows one to study the effects at the various discontinuities of the applicator–catheter–tissue system and gives a better understanding of known phenomena.**

I. Introduction

More than a decade ago, it became apparent that the use of microwave and radio-frequency applicators is a reliable method for effective heating of malignant tumors [14]. Especially for deep-seated tumors, hyperthermia applied by interstitial applicators proved to be effective as an adjuvant therapy with brachytherapy [4].

When designing interstitial antennas, the main objectives are to deposit energy in a well-defined tumor volume in order not to damage normal tissue, and also to achieve a good impedance match.

Several attempts have been made to calculate analytically the EM-field in the vicinity of such an antenna [2], [7], [9], [15], [20], [21] and also to investigate their input impedance [19]. Because of the complicated structure of interstitial antennas, together with the surrounding catheter, a lot of simplifications have been necessary to perform the calculations.

It is the purpose of this paper to avoid these simplifications and to model interstitial antennas and catheters as realistically as possible and then to apply numerical solutions. This is done using the field evaluation program MAxwell's equations using the Finite Integration Algorithm (MAFIA) [1], [17], and [18]. The result is a precise pattern of the E-field distribution inside the coaxial line as well as in the catheter, and, of course most interestingly, in the lossy tissue. From these field distributions both SAR-distributions in tissue and standing wave patterns inside the coaxial line, and therefore the impedance match, can be derived easily.

At present, microwave antennas used in clinical routine [8], [10], and [16] often consist of a semirigid coaxial cable with an extension of the inner conductor for a length of a few centimeters. The diameter of the cables is small enough to fit the catheters which are normally needed for the insertion of radioactive seeds in brachytherapy.

Investigating interstitial applicators rigorously means that the whole system antenna-catheter-tissue must be taken into account. For example neglecting the catheters leads to erroneous results. The main reason for this is that the outer conductor of the semi-rigid line is the inner conductor of a new coaxial line. Its lossy outer conductor is formed by the surrounding tissue and its dielectric is the catheter between these conductors. Using conventional coaxial applicators, a relatively strong wave propagates backward in this line from the junction of the applicator to the generator, seeing approximately an open end at the inlet of the applicator into tissue, which leads to an enhancement of the electric field at this point and therefore to a local maximum of the SAR-distribution.

In clinical practice of interstitial hyperthermia, physicians try to keep pain away from the patient when they empirically use a mold technique: tissue equivalent material is put on the skin of the treated patient and around the catheter inlets of the antennas. The consequence is that the local SAR maximum is formed in the mold and no more on the skin.

In order to interrupt currents at the surface of the applicators, $\lambda/4$ chokes have been proposed and investigated experimentally [6], [11], [19]. Simulations of these types of applicators as well as of conventional ones are presented in this paper.

In certain applications, when the insertion depth of the catheters is limited, a so called "end-fire"-characteristic is desirable [3], [12]. A principal way to achieve this, and also to concentrate power deposition in a smaller volume, is to shorten the dipoles, however, without disturbing the impedance match. This can be achieved with a dielectric load having a high relative permittivity (e.g., $\varepsilon_r = 100$).

In many hyperthermia sessions, interstitial applicators are not applied alone but in the form of antenna arrays with a spacing of about 1–2 cm between the antennas [22]. In these cases one should take care of the phases of the input signals supplying the applicators. Normally in-phase signals are applied which have the potential for a local SAR-maximum between the applicators. Simulation results for a 2×1-antenna array and a 2×2-antenna array are also presented in the following sections.

Manuscript received August 31, 1995; revised February 15, 1996. This work was supported in part by the Deutsche Forschungsgemeinschaft (DFG): Fi 371/2-1 and Se 525/4-2, by the Sofie Wallner Foundation Erlangen, and by the Johannes and Frieda Marohn Foundation at the University of Erlangen-Nürnberg.

The authors are with the Laboratories for High Frequency Technology, University Erlangen-Nürnberg, Cauerstr. 9, 91058 Erlangen, Germany.

J. Erb is also with the Department of Radiation Oncology, University Erlangen-Nürnberg, Universitätsstraße 27, 91054 Erlangen, Germany.

Publisher Item Identifier S 0018-9480(96)03787-8.

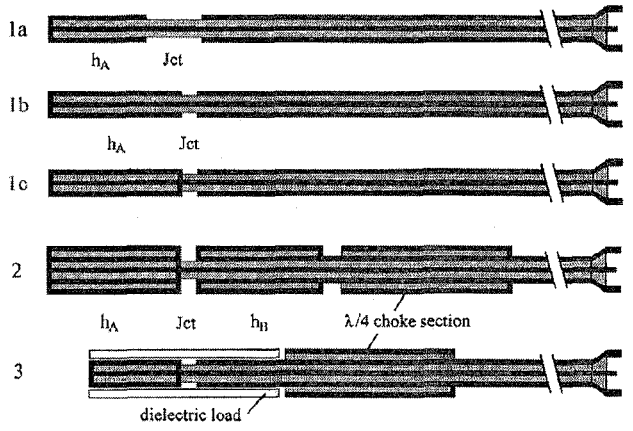

Fig. 1. Types of antennas under investigation:Coaxial [1(a), (b), and (c)] and triaxial designs (2 and 3) with $\lambda/4$ choke section.

II. Models

A survey of the antennas under investigation is given in Fig. 1. For experiments the conventional applicators [Type 1(a), (b), and (c)] are made of commercially available semi-rigid coaxial lines: Type UT-47 from UTI, Micro-Coax Components, Collegeville, PA 19426. The center conductor (diameter: 0.30 mm) consists of silver plated copper-weld steel (SPCW). It is concentrically surrounded by the dielectric (diameter: 0.95 mm) which is made of polytetrafluorethylen (PTFE). The relative permittivity of PTFE is ε_r =2.03. The outer conductor (diameter: 1.19 mm) consists of a seamless tubular copper jacket.

The triaxial semi-rigid coaxial cable, type UT 78-50-25, also from UTI, is needed for the construction of antennas for the modified type 2 and type 3 applicator in Fig. 1. The center conductor (diameter: 0.20 mm) consists again of SPCW. It is concentrically surrounded by the inner dielectric (diameter: 0.66 mm) which is PTFE. The inner conductor (diameter: 0.86 mm) and the outer conductor (diameter: 1.98 mm) consist of seamless tubular copper jackets. Between the inner and the outer conductor, there is the second PTFE dielectric layer (diameter: 1.47 mm). This triaxial cable is able to transport a maximum average power of 24.5 W (CW) at 915 MHz in its inner coaxial line. This is a good compromise between a minimum in diameter and a maximum of possible power transfer.

Suitable insulating brachytherapy catheters are chosen for the coaxial and triaxial antennas. All catheters consist of PTFE. The sheath for the coaxial line is 1.2 mm in inner diameter and has a wall thickness of 0.3 mm. Comparable sheaths are chosen for the triaxial antennas: Inner diameter here is 2.0 mm and wall thickness is 0.5 mm.

All calculations are based on mesh grids which fit the physical dimensions of the semi-rigid cables and catheters as good as possible, but always include the intention to obtain an acceptable CPU-time. According to the regions of interest the grid dimensions are varied between 10–100 nodes per cm in all directions. In case of single antenna simulations, the rotational symmetry can also be used favorably to apply a quasi-two–dimensional (2-D) simulation.

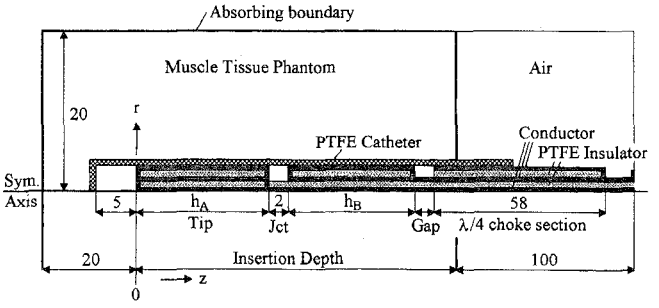

Fig. 2. Model for simulation of a triaxial interstitial dipole antenna (Fig. 1: Type 2) with PTFE catheter radiating into muscle tissue (MT)(dimensions in mm).

For simulations the environment of the applicator is as important as its structure. In Fig. 2 the model of the applicator–catheter–tissue system is given in detail (not to scale). Besides the structure and the dimensions of the applicator and the catheter, and, of course, the electrical parameters of all materials, the other critical parameter is the insertion depth, especially for conventional designs [Type 1(a), (b), and (c)].

The electrical properties of the simulated muscle tissue phantom at 915 MHz are chosen as follows: relative permittivity $\varepsilon_r = 50$ and conductivity $\sigma = 1.2$ S/m. The volume of the muscle tissue phantom is limited by absorbing boundaries at a distance of 20 mm from the symmetry axis (SA) to avoid unnecessary computations. At this distance the field components are weak enough to justify this restriction. Losses in the coaxial cables as well as in the catheter are neglected in the simulations, since they are much smaller than those in muscle tissue.

All simulations given here have been completed on HP 720 workstations.

III. Simulations

Important features and properties of interstitial dipole applicators are described and compared in this section. The main effort is on the comparison of calculated return loss and distributions of the specific absorption rate (SAR).

A few details of the "microscopic behavior" of the E-field at various discontinuities of the applicators are also presented, which give a deeper insight and a better understanding of what happens inside and near those relatively complicated structures. These details may lead to further improvements and optimization of interstitial microwave applicators.

IV. Reflection Coefficient

An important prerequisite for an useful applicator design is that the power delivered by the generator is transported to and absorbed in the tissue. This can be guaranteed by the use of low-loss cables and catheters, but especially by the use of a proper antenna design which leads to a high return loss when the antenna is connected to the normally used 50 Ω-systems.

In principle, nearly ideal match at the operating frequency can be achieved using tuners (e.g., stub tuners) distant from the antenna. One severe disadvantage of such a system is the complicated handling and the possible high voltage standing

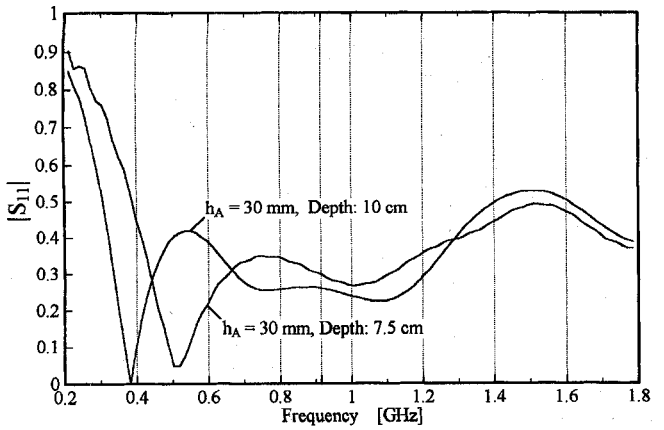

Fig. 3. Calculated $|S_{11}(f)|$ of a closed coaxial dipole antenna [Fig. 1: Type 1(c)]with different insertion depths: 7.5 cm and 10.0 cm.

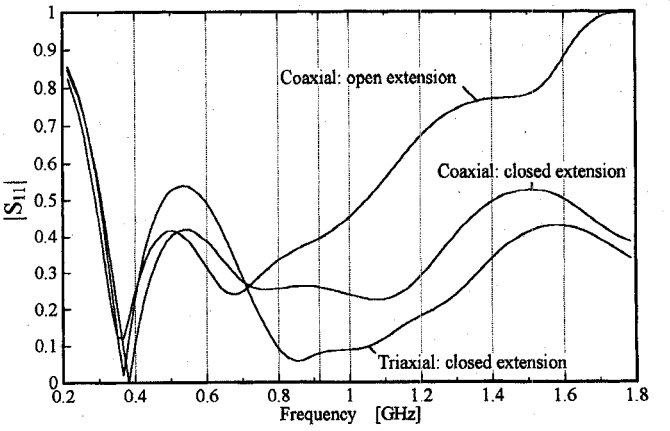

Fig. 4. Comparison of calculated $|S_{11}(f)|$ of a coaxial dipole antenna with an open extension [Fig. 1: Type 1(b)], a coaxial dipole antenna with a closed extension [Fig. 1: Type 1(c)], and a triaxial dipole antenna (Fig. 1: Type 2) with a $\lambda/4$ choke section. In all types antenna tip length h_A is 30 mm and insertion depth is 10.0 cm.

wave ratio (VSWR) on the antenna cable which leads to increased conductor losses. Another disadvantage of using stub tuners within antenna arrays is that the phases of the antennas are changed. This may cause focusing of energy to unexpected locations. To avoid these disadvantages the return loss should not be less than about R $\approx$ 10 dB, corresponding to a reflection coefficient of $|S_{11}| \approx 0.32$ or a VSWR of about 2 : 1.

Consequently, proper return loss should be the first design goal before investigating E-field and SAR distributions.

The first design step is the optimization of the dipole lengths of the antenna type 2 in Fig. 1 ($h_A = h_B$). The reason for this is that the return loss of the coaxial models [types 1(a), (b), and (c)] depends on the insertion depth, and that it is quite impractical to optimize these applicators for distinct insertion depths. The result of this optimization process for a small reflection coefficient at 915 MHz is $h_A = h_B = 30$ mm. This dipole half length is also used for the conventional dipole type 1(c) and the modified type 1(b) of Fig. 1, too. Type 1(b) differs from type 1(c) only in that 1(c) has a "closed" h_A-segment (closed coaxial antenna) and 1(b) has an "open" h_A-segment (open coaxial segment) near the junction (Jct).

Return loss functions for antennas of type 1(c) (closed coaxial antennas) with two different insertion depths are shown in Fig. 3. It can be seen that the reflection depends on the insertion depth. Especially at the normal operating frequency of 915 MHz the reflection coefficient increases from 0.25 to 0.3 when decreasing the insertion depth from 10 cm to 7.5 cm. In general, calculated $|S_{11}(f)|$ at various other insertion depths indicates a great variation at 915 MHz. Already this result indicates that an electromagnetic field extends to the inlet of the applicator into the body. This effect will be further investigated within the next sections.

The fact that the frequency of the first minimum strongly depends on the insertion depth also becomes quite evident. In the examples given here, this is indicated by minima at 380 MHz and 510 MHz with insertion depths of 10 cm and 7.5 cm, respectively.

A similar comparison for the antennas of type 1(b), type 1(c) and type 2 is given in Fig. 4 with an insertion depth of 10 cm for all three antennas. It can be seen that all antennas show the first $|S_{11}|$ minimum at approximately the same frequency

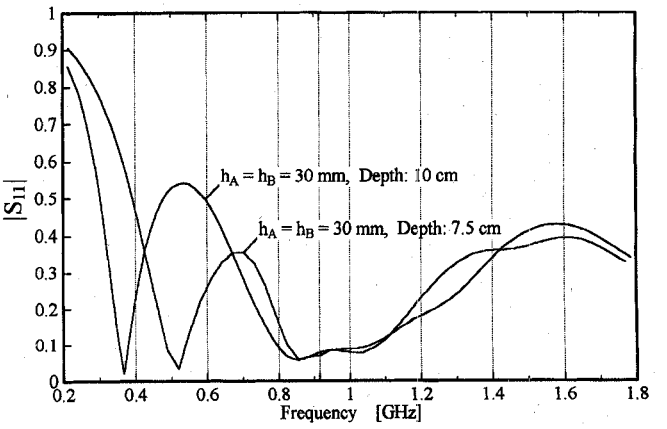

Fig. 5. Calculated $|S_{11}(f)|$ of a triaxial dipole antenna (Fig. 1: Type 2) with $\lambda/4$ choke section with different insertion depths: 7.5 cm and 10.0 cm.

(380 MHz). Moreover, the optimized triaxial antenna (type 2) exhibits an excellent return loss of more than R = 20 dB at 915 MHz.

In order to achieve an optimum antenna performance, the choke is separated from the dipole. In contrast to a construction given in [19], where the choke is folded into one half of the dipole, this design leads to an additional parameter for optimization.

The effect of the choke in the triaxial structure of type 2 antenna is demonstrated in Fig. 5. Like the coaxial types before, $|S_{11}|$ depends on the insertion depth, except for the operating frequency. This is a proof for the effectiveness of the $\lambda/4$ choke, which has been designed for 915 MHz, and it is also a hint for the SAR-distribution to be concentrated around the dipole, independent of different insertion depths. Also this effect is investigated in greater detail within the next sections.

In clinical practice sometimes slightly different catheters are used for implantation in the patient. Therefore, the influence of the wall thickness on the applicators should be known. The influence on applicators of type 2 is given in Fig. 6 for wall thicknesses of 0.3 mm and 0.5 mm. Despite the fact that $|S_{11}(f)|$ is nearly doubled at 915 MHz for a wall thickness of 0.3 mm, the absolute value is still acceptable.

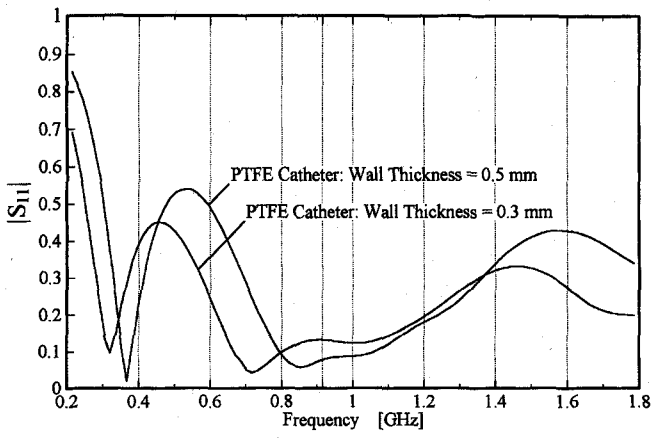

Fig. 6. Calculated $|S_{11}(f)|$ of a triaxial dipole antenna (Fig. 1: Type 2) with $\lambda/4$ choke section using different PTFE Catheters: Wall thicknesses are 0.5 mm and 0.3 mm.

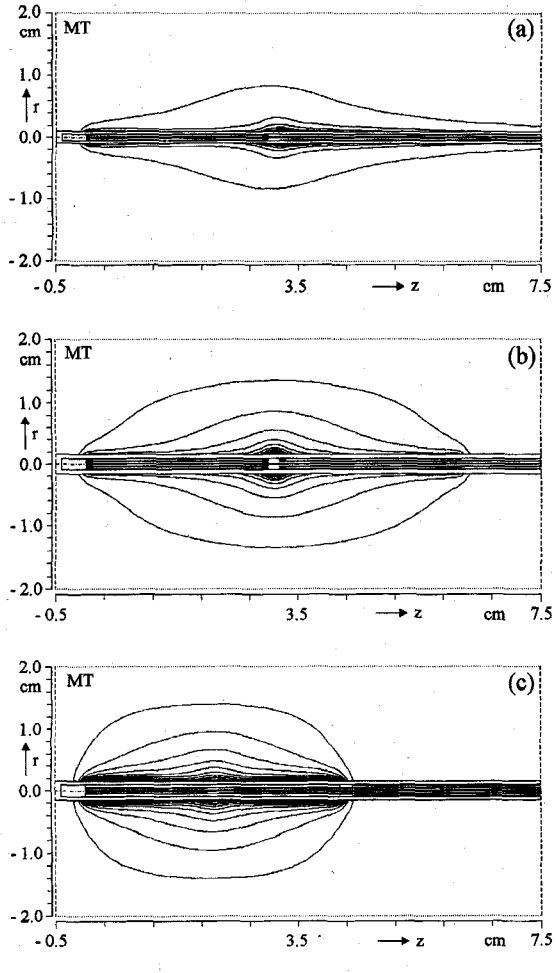

Fig. 7. Calculated iso-SAR contour lines of different applicator types: (a) closed coaxial dipole antenna [Fig. 1: Type 1(c)], (b) triaxial dipole antenna with $\lambda/4$ choke section (Fig. 1: Type 2), and (c) triaxial dipole antenna with dielectric load and $\lambda/4$ choke section (Fig. 1: Type 3). All antennas are immersed in muscle tissue at an insertion depth of 10 cm.

Another important parameter, which is not investigated in this paper, is the influence of the tissue on $|S_{11}(f)|$. Here, an exact knowledge of the permittivity and conductivity is assumed. On the other hand, if a well-defined applicator is available, one could think of deriving tissue parameters from $|S_{11}(f)|$ curves.

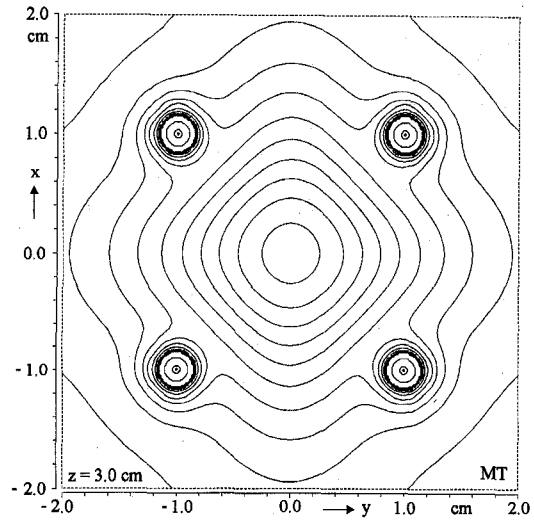

Fig. 8. Calculated iso-SAR contour lines of four triaxial dipole antennas (Fig. 1: Type 2; Jct = 2 mm, dipole half lengths $h_A = h_B = 30$ mm) at an insertion depth of 7.5 cm radiating in phase into muscle tissue. A cut through the array near the junctions of the antennas at $z = 3.0$ cm is shown. The thickness of the catheters is 0.5 mm.

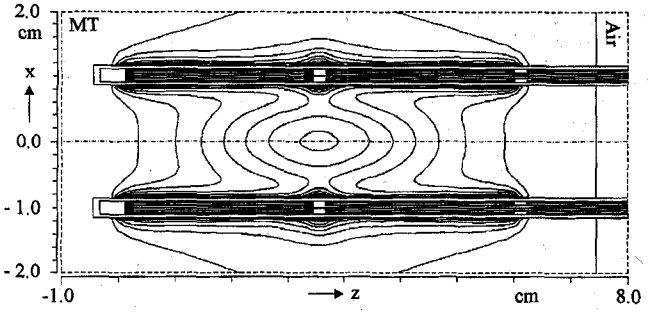

Fig. 9. Calculated Iso-SAR contour lines of four triaxial dipole antennas (Fig. 1: Type 2; Jct = 2 mm, dipole half lengths $h_A = h_B = 30$ mm) at an insertion depth of 7.5 cm radiating in phase into muscle tissue. A cut in xz-plane through the antenna array (Distance from the center of the antenna array: $y = 1.0$ cm) is shown. The thickness of the catheters is 0.5 mm.

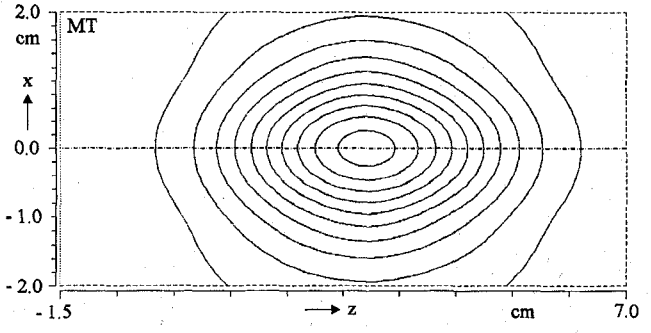

Fig. 10. Calculated Iso-SAR contour lines of four triaxial dipole antennas (same conditions as in Fig. 9). A cut in xz-plane through the center of the antenna array ($y = 0.0$ cm) is shown.

V. SAR Pattern

The purpose of a hyperthermia session is to heat a defined tumor volume. Power should be mainly dissipated in this volume to achieve this goal. So the objective is to design antennas with a given antenna pattern, or, to be more specific, with

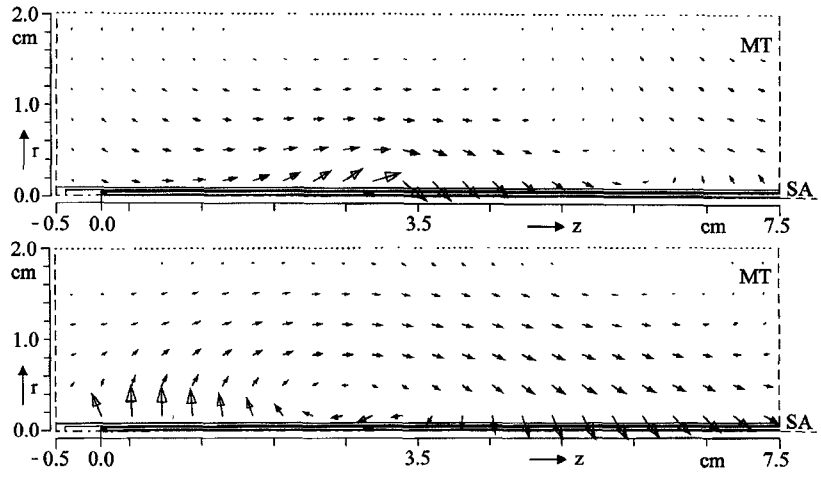

Fig. 11. Instantaneous views of the E-field distributions of a closed coaxial dipole antenna [Fig. 1: Type 1(c)] with an insertion depth of 10 cm radiating into muscle tissue (MT) [symmetry axis (SA)]. Two time steps are shown for $t = 0$ (upper diagram) and $t = T/4$ (lower diagram).

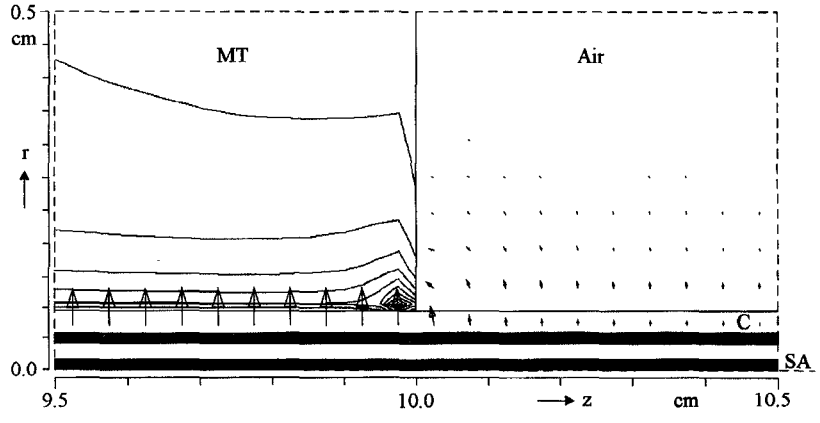

Fig. 12. Instantaneous view of the E-field and calculated SAR distribution at the interface between muscle tissue and air for a closed coaxial dipole antenna [Fig. 1: Type 1(c)]. [Symmetry axis (SA), Catheter (C) and Muscle Tissue (MT)].

a given SAR pattern. For example, applicators whose SAR patterns vary with the insertion depth are highly undesirable. This is exactly the case for the antennas of type 1.

A basic dilemma with interstitial applicators is that the length of the dipoles is limited in most cases for practical reasons, and that, on the other hand, the penetration depth must not be too small. Often the ISM frequency of 915 MHz is a good compromise between these diverging demands. Hence, the SAR patterns are calculated for this frequency.

If the longitudinal extent of the SAR-pattern should be concentrated, the dipoles can be shortened by means of a dielectric shell with a high permittivity. For a thin dielectric pod with a permittivity of $\varepsilon_r = 100$ the optimized length for a minimum reflection coefficient at 915 MHz has been found to be $h_A = h_B = 20$ mm (type 3 of Fig. 1). In Fig. 7(c) the iso-SAR lines of this applicator compared with those of type 1(c) [Fig. 7(a)] and type 2 [Fig. 7(b)] are given. The lines are normalized to the absolute maximum value which is taken to be 100%, they are decreased in steps of 10%.

The effectiveness of the choke, which has been already supposed from the $|S_{11}(f)|$-curves is clearly demonstrated for applicator type 2 [Fig. 7(b)]. This is also the case for the dielectrically loaded applicator type 3 [Fig. 7(c)].

As was already pointed out, most of the tumor volumes require the application of more than one interstitial antenna. Therefore, it is advantageous to take the principles of phased arrays into consideration, too. Feeding the applicators with equal-phased signals may lead to significant SAR-enhancements between the applicators compared with applicators fed with arbitrary phases.

In Fig. 8 a cross sectional cut, in Fig. 9 a longitudinal cut through two triaxial dipole antennas and in Fig. 10 a longitudinal cut through the center of a 2 × 2 triaxial dipole antenna array are given. The SAR value in the array center Fig. 8 and Fig. 10 relative to the absolute SAR maximum near the antennas' junctions is 60%.

VI. E-Field Pattern

The study of the electromagnetic field in the antenna-catheter-tissue system is not only of academic interest, it may also lead to consequences for the practical design of applicators. Some of the simulated effects shown in this paper are hard to verify experimentally. Regular E-field probes are often too large to detect steep field gradients and the measured signal represents only a field averaged over several

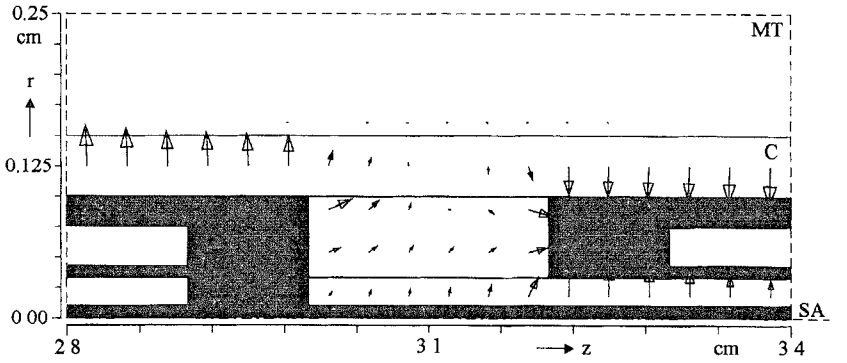

Fig. 13. Instantaneous view of the E-field distribution near the junction (Jct = 2 mm) of a triaxial dipole antenna (Fig 1: Type 2) [Symmetry Axis (SA), Catheter (C), and Muscle Tissue (MT)].

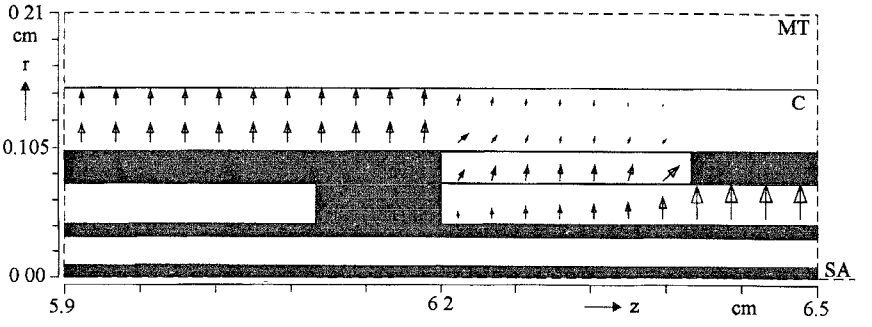

Fig. 14 Instantaneous view of the E-field distribution near the gap (gap length = 2 mm) and $\lambda/4$ choke section of a triaxial dipole antenna (Fig. 1: Type 2). [Symmetry Axis (SA), Catheter (C), and Muscle Tissue (MT)].

millimeters. Another problem is that it is rather impossible to place E-field probes inside the junction or the catheter.

Fig. 11 shows the vectors of the electrical field in muscle tissue at two different moments with a time interval of $T/4$ in between, where T is the temporal period, for a dipole antenna of type 1(c) at 915 MHz. The arrows indicate the direction and the strength of the field at their starting points.

Except for the junction, strong radial components can be seen near the catheter with a strong gradient near the antenna's tip. A half-wave-length of about 6 cm also reveals the dominant influence of the catheter with its low permittivity.

A close-up of the puncture of the applicator into the tissue is given in Fig. 12 for an antenna of type 1(c). In this figure, the E-field in the catheter and in the air is shown. The presentation of E-field vectors in the feeding line is suppressed because of graphical reasons. Additionally, the calculated SAR-distribution in muscle tissue is added. As mentioned before, a "coaxial wave" is propagating along the applicator backward to the inlet. This wave is nearly totally reflected at the tissue-air interface. The result is a standing wave and an important local SAR-maximum ("hot spot") at the puncture, as can be seen in Fig. 12.

Figs. 13 and 14 show details of the field distribution in the vicinity of the junction and of the open end of the $\lambda/4$ choke section, both for the type 2 applicator. Again, the coaxial line character of the outer conductor-catheter-tissue system is evident as is the effectiveness of the $\lambda/4$ choke section. Of course, the minuteness of the field in the tissue is not mainly caused by the radial decay because of geometrical reasons, but is due to the electrical properties of catheter and tissue.

Finally, Fig. 15 shows an instantaneous view of the E-field distribution for a 2×1 antenna array [Fig. 1: Type 1(a)] in a longitudinal cut. The field enhancement in the tissue between the applicators (h_A = 10 mm, Jct = 5 mm) is evident.

VII. Experiments

Simulation results are compared with experimental data from SAR measurements performed with a computer controlled 3-axis scanning system, where E-field probes are driven by automatic stepper motors in a liquid muscle phantom [13]. PTFE catheters described above are installed perpendicular to the phantom fluid surface between two lucite plates. The antennas to be characterized are inserted and fixed into the catheters at the desired insertion depths. A 40 dm^3 lucite box is filled with a homogeneous phantom fluid consisting of 70.0% ethanediol, 28.0% H_2O and 2.0% NaCl (weight percents). The dielectric properties are equivalent to high water content tissue (ε_r = 50 and σ = 1.2 S/m) at 915 MHz and room temperature [5].

The E-field probe used (Fig. 16) consists of an Al_2O_3-substrate (0.635 mm thickness), on each side two resistive chrome-nickel-lines are connected to a gold-dipole. The CrNi-lines have a thickness of less than 1 μm and are 80 μm wide. The distance between the lines is 100 μm. The lines are quasitransparent for RF-fields because of their small dimensions and high resistivity (800 kΩ/m). Two miniature beam-lead

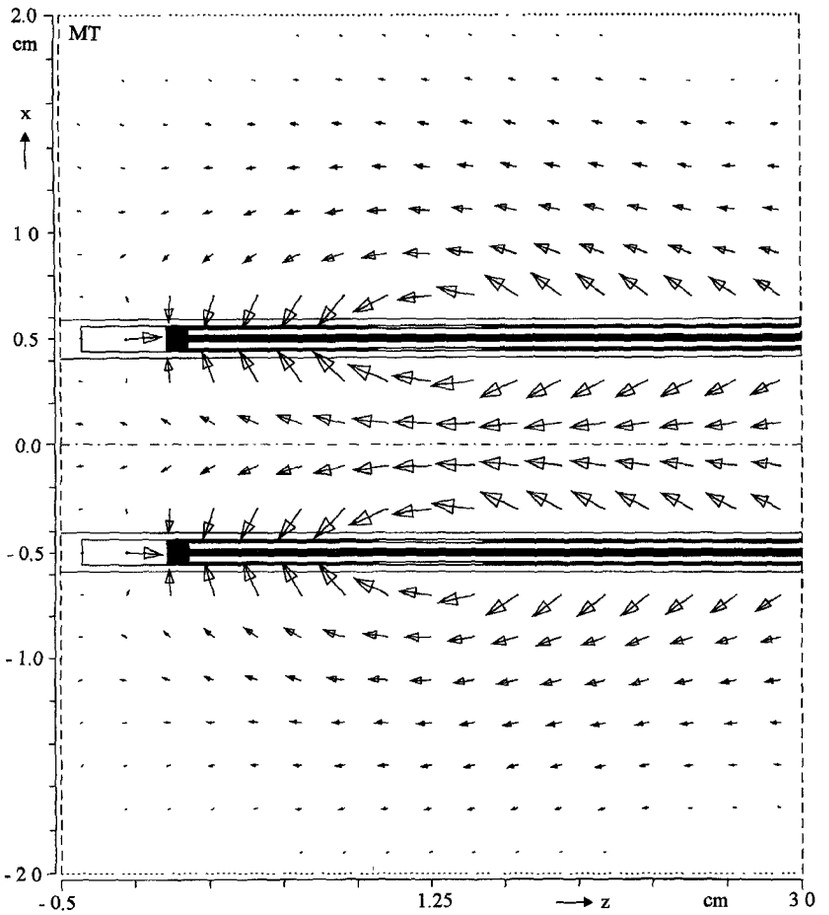

Fig. 15. *Instantaneous* view of the E-field distribution between two coaxial dipole antennas [Fig. 1: 1(a); Jct ≈ 5 mm, antenna tip length h_A is 10 mm] with an insertion depth of 5 cm radiating in phase into muscle tissue. The thickness of the catheters is 0.3 mm.

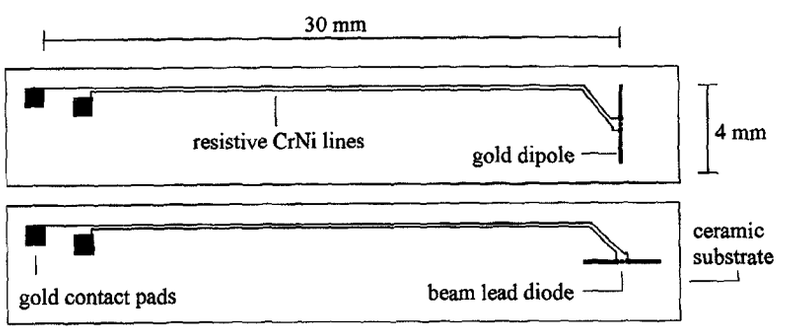

Fig. 16. E-field probe with orthogonal dipoles on the front and back side of a ceramic substrate.

Schottky-diodes (BAT 15-110 S) complete the circuits on each side of the substrate. The gold-dipoles are centered perpendicular to each other to be able to measure two field components simultaneously. For performance purposes the diodes are biased with 4.6 μA. The probe is isolated by a special varnish to avoid direct contact with the conductive phantom fluid.

The amplitude of the received demodulated RF signal is proportional to $|\mathbf{E}|^2$ and according to its definition directly proportional to the specific absorption rate (SAR), when using a homogeneous medium where σ and ρ are constant.

Experimental results of 3D-SAR-measurements are shown in Figs. 17 and 18. The relative SAR-distributions of a clinically used interstitial coaxial applicator [type 1(b)] and of a triaxial dipole antenna (type 2), both with an insertion depth of 12 cm, are compared. Due to the discussed effect of a wave traveling along the outer conductor backward to the generator, the SAR pattern of the coaxial type antenna is enlarged toward the inlet. The triaxial antenna with $\lambda/4$ choke section, however, has a symmetrical SAR pattern situated around the junction.

When comparing experimental and simulated results (Fig. 7), the experimental relative SAR patterns (e.g., the position of 10%-iso-SAR line) appear broader than the simulated ones. This is due to the impossibility to measure the steep E-field gradient in the vicinity of the antenna. This means

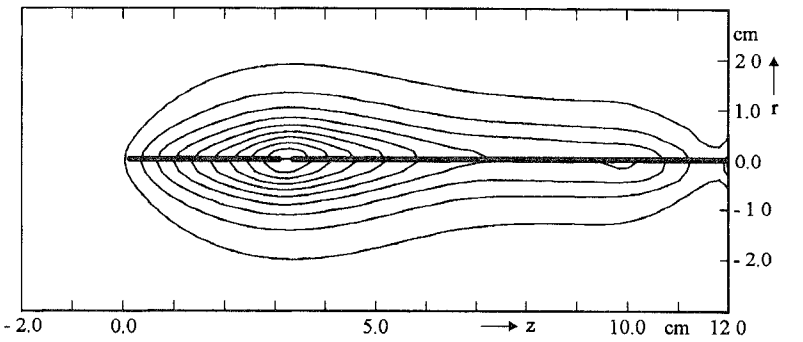

Fig. 17. Measured SAR pattern of a coaxial antenna [Type 1(b)] at 915 MHz Additionally the shape and the position of the dipole antenna with an insertion depth of 12 cm is drawn. The 10–90%-iso-SAR lines are plotted.

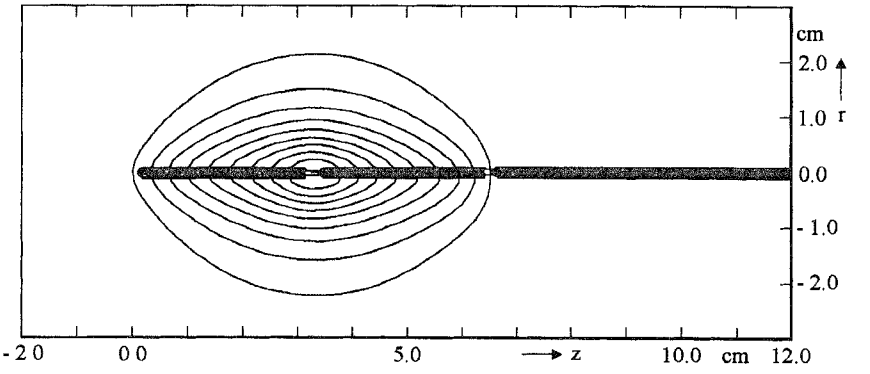

Fig. 18. Measured SAR pattern of a triaxial dipole antenna with $\lambda/4$ choke section (Type 2) at 915 MHz. Additionally the shape and the position of the dipole antenna with an insertion depth of 12 cm is drawn. The 10–90%-iso-SAR lines are plotted.

that the total SAR-maximum measured by the E-field probe is far lower than that evaluated in the simulation. Therefore, the relative decay of E-field strength in the experiment is not as steep as it is in the simulation.

A comparison of simulated and experimental results for the return loss is given in [13].

VIII. Conclusion

The described procedure allows a quick and precise evaluation of applicators for interstitial microwave hyperthermia. Particularly, the applied method does not suffer from some restrictions, neither geometrical nor electrical, as do the approximate analytical approaches. For example, the case of shortening dipoles (type 3 of Fig. 1) by means of a dielectric load (permittivities of applicator or catheter are greater than the surrounding tissue) can be handled, whereas the theoretical analysis in [2], [9], and [19] cannot.

The most important features are the possibilities to calculate the SAR-distribution around the applicator and to verify the impedance match of the applicator at the same time.

A few important conclusions are the following:

- The specification of applicators alone makes no sense. The whole applicator-catheter-lossy tissue system has to be considered.
- Conventional coaxial applicators lack a predefined SAR-pattern and a predefined reflection coefficient at the operating frequency. Here the insertion depth is the critical parameter when using these types of applicators. Furthermore, "hot spots" and consequently burns are possible at the puncture.
- As was shown experimentally, for example in [6], a $\lambda/4$ choke section is a powerful means to avoid waves propagating backward on the outer conductor. Triaxial applicators are desirable also when thinking of a specific reflection coefficient at the operating frequency.
- The applicators under investigation show strong radial E-field components close to their tip. In many cases these strong field gradients cannot be verified experimentally because field probes normally integrate signals over several millimeters.
- It is more complicated to shift the maximum of the SAR toward the antenna's tip than to achieve a smooth pattern in an extended volume. One method to gain the first design goal is to load a dipole dielectrically. The latter can be realized, for example, by a multiple junction design or by lower operating frequencies with the further advantage of a higher penetration depth.

Paying attention to some inevitable physical restrictions, the applied simulation method allows the individual design of interstitial antennas for a large number of clinical applications.

References

[1] M. Bartsch *et al.*, "Finite integration: ein universell anwendbares verfahren zur berechnung elektromagnetischer felder," *VDE-Fachbericht*, vol. 45, p 109, 1993.

[2] J. P Casey and R. Bansal, "The near field of an insulated dipole in a dissipative dielectric medium," *IEEE Trans Microwave Theory Tech.*, vol. 34, no. 4, p. 459, 1986.

[3] G. Cerri, R. De Leo, and V. M. Primiani, "'Thermic end-fire' interstitial applicator for microwave hyperthermia," *IEEE Trans. Microwave Theory Tech.*, vol. 41, no. 6/7, p. 1135, 1993.
[4] C. T. Coughlin, T. Z. Wong, J. W. Strohbehn, T. A. Colacchio, J. E. Sutton, R. Z. Belch, and E. B. Douple, "Intraoperative interstitial microwave-induced hyperthermia and brachytherapy," *Int. J. Radiat. Oncol. Biol. Phys.*, vol. 11, p. 1673, 1985.
[5] J. Erb, G. Schaller, H. M. Seegenschmiedt, and R. Sauer, "Characterization of semirigid coaxial antennas for interstitial and endocavitary microwave hyperthermia," *Europ. J. Phys. Med. Rehab.*, vol. 4, no. 2, p. 52, 1994.
[6] W. Hürter, F. Reinbold, and W. J. Lorenz, "A dipole antenna for interstitial microwave hyperthermia," *IEEE Trans. Microwave Theory Tech.*, vol. 39, no. 6, p. 1048, 1991.
[7] M. F. Iskander and A. M. Tumeh, "Design optimization of interstitial antennas," *IEEE Trans. Biomed. Eng.*, vol. 36, no. 2, p. 238, 1989.
[8] K. M. Jones, J. A. Mechling, J. W. Strohbehn, and B. S. Trembly, "Theoretical and experimental SAR distributions for interstitial dipole antenna arrays used in hyperthermia," *IEEE Trans. Microwave Theory Tech.*, vol. 37, no. 8, p. 1200, 1989.
[9] R. W. P. King, B. S. Trembley, and J. W. Strohbehn, "The electromagnetic field of an insulated antenna in a conducting or dielectric medium," *IEEE Trans. Microwave Theory Tech.*, vol. 31, no. 7, p. 574, 1983.
[10] T. P. Ryan, "Comparison of six microwave antennas for hyperthermia treatment of cancer: SAR results for single antennas and arrays," *Int. J. Radiat. Oncol. Biol. Phys.*, vol. 21, p. 403, 1991.
[11] T. P. Ryan, J. Mechling, and J. W. Strohbehn, "Absorbed power deposition for various insertion depths for 915 MHz interstitial dipole antenna arrays: experiment versus theory," *Int. J. Radiat. Oncol. Biol. Phys.*, vol. 19, no. 2, p. 377, 1990.
[12] V. Sathiaseelan, L. Leybovich, B. Emami, P. Stauffer, and W. Straube, "Characteristics of improved microwave interstitial antennas for local hyperthermia," *Int. J. Radiat. Oncol. Biol. Phys.*, vol. 20, no. 3, p. 531, 1991.
[13] G. Schaller, J. Erb, and R. Engelbrecht, "Field simulation of applicators for interstitial microwave, hyperthermia," in L. Kirby, Hrsg., in *Proc. IEEE MTT-S Int. Microwave Symp.*, Orlando, FL, May 15–19, 1995, p. 307.
[14] J. W. Strohbehn, T. C. Cetas, and G. M. Hahn, "Special issue on HT and cancer therapy-guest editorial," *IEEE Trans. Biomed. Eng.*, vol. 31, no. 1, p. 1, 1984.
[15] B. S. Trembly, "The effects of driving frequency and antenna length on power deposition within a microwave antenna array used for hyperthermia," *IEEE Trans. Biomed. Eng.*, vol. 32, no. 2, p. 152, 1985.
[16] A. M. Tumeh and M. F. Iskander, "Performance comparison of available interstitial antennas for microwave hyperthermia," *IEEE Trans. Microwave Theory Tech.*, vol. 37, no. 7, p. 1126, 1989.
[17] T. Weiland, "Die diskretisierung der maxwell-gleichungen," *Phys. Bl.*, vol. 42, no. 7, p. 191, 1986.
[18] ——, *MAFIA Version 3.2-The ECAD System-Userguide,* The MAFIA Collaboration, Ohlystraß 69, 64285 Darmstadt, 1994.
[19] T. Z. Wong and B. S. Trembly, "A theoretical model for input impedance of interstitial microwave antennas with choke," *Int. J. Radiat. Oncol. Biol. Phys.*, vol. 28, no. 3, p. 673, 1994.
[20] Y. Zhang, N. V. Dubal, R. Takemoto-Hambleton, and W. T. Joines, "The determination of the electromagnetic field and SAR pattern of an interstitial applicator in a dissipative dielectric medium," *IEEE Trans. Microwave Theory Tech.*, vol. 36, no. 10, p. 1438, 1988.
[21] Y. Zhang, W. T. Joines, and J. R. Oleson, "The calculated and measured temperature distribution of a phased interstitial antenna array," *IEEE Trans. Microwave Theory Tech.*, vol. 38, no. 1, p. 69, 1990.
[22] ——, "Microwave hyperthermia induced by a phased interstitial antenna array," *IEEE Trans. Microwave Theory Tech.*, vol. 38, no. 2, p. 217, 1990.

Gerd Schaller received the diploma in electrical engineering from the Technische Hochschule, Munich, Germany, in 1965 and the Dr.-Ing. degree from the University of Erlangen-Nuremberg, Germany in 1976.

From 1966–1969, he worked at Grundig Electronics as a Research and Development Engineer on the design and development of electro-optical components and systems. In 1969, he joined the Laboratories for High Frequency Technology at the Univ. of Erlangen-Nuremberg. His research activities have been in the area of microstrip components and microwave radiometry. Currently his research interest is in the application of microwaves for medical purposes, including especially interstitial microwave hyperthermia.

Jurgen Erb was born in Fürth/Bavaria, Germany, in 1965. He received the diploma in physics (Dipl.-Phys.) in 1991, and the Ph.D. degree (Dr. rer. nat.) in physics from the University of Erlangen-Nuremberg in 1995.

Since 1992, he has been working as a certified Medical Physicist (DGMP) with the Dept. of Radiation Oncology, and as a Research Associate with the Laboratories for High-Frequency Technique, both at the Univ. of Erlangen-Nuremberg. He has done research work on Solid State Physics (high temperature superconductors) and Medical Physics (brachytherapy, dosimetry, radiation protection, and applicator development for interstitial hyperthermia). Presently, his main research interests deal with the development and application of model-based treatment planning software for both radiation therapy and microwave hyperthermia.

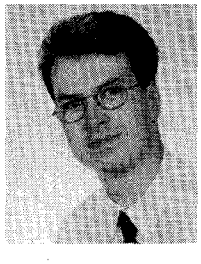

Rainer Engelbrecht was born in Schweinfurt, Germany, in 1969. He received the M.S.E.E. degree (Dipl.-Ing.) from the University of Erlangen-Nuremberg, Germany, in 1995. Currently, he is pursuing the Ph.D. degree (Dr.-Ing.) at the Laboratories for High Frequency Technology at the Univ. of Erlangen-Nuremberg, Germany.

Since 1992, he has been working on medical RF and microwave applications for therapy, diagnostics and safety. His research interests are in theoretical and experimental investigations on microwave excited gas lasers.